Fabrication and Optical Properties of Er 2-x Yb x Zr 2 O 7 Transparent Ceramics

Ting Deng
southwest university of science and technology
Kuibao Zhang (xiaobao320@163.com)
Kui Liu
Southwest University of Science and Technology
Jianjun Zeng
Southwest University of Science and Technology
Daimeng Chen
Southwest University of Science and Technology
Haiyan Guo
Southwest University of Science and Technology

Research Article

Keywords: transparent ceramics, luminescence, energy transfer, Er2-xYbxZr2O7-

Posted Date: August 26th, 2020

DOI: https://doi.org/10.21203/rs.3.rs-64824/v1

Fabrication and optical properties of $Er_{2-x}Yb_xZr_2O_7$ transparent ceramics

Ting DENG [a], Kuibao ZHANG [a,b]*, Kui LIU [a], Jianjun ZENG [a], Daimeng CHEN [a], Haiyan GUO [a]

[a] State Key Laboratory of Environment-friendly Energy Materials, Southwest University of Science and Technology, Mianyang, Sichuan 621010, China.

[b] Fundamental Science on Nuclear Wastes and Environmental Safety Laboratory, Southwest University of Science and Technology, Mianyang 621010, China.

*Corresponding Author: xiaobao320@163.com

Tel./Fax: +86-816-2419492

Abstract: In this study, transparent $Er_{2-x}Yb_xZr_2O_7$ (x = 0-2.0) ceramics were successfully prepared by vacuum sintering at 1850 °C for 6 h. The phase composition, microstructure evolution and optical transmittance of the transparent ceramics were investigated. The powders and ceramics demonstrate a single-phase defective fluorite structure. All the ceramics exhibit excellent optical performance and the highest transmittance can reach to 76% at 1100 nm when x=1.0. The upconversion and infrared emission under 980 nm exciting were measured and discussed as well. The $Er_{2-x}Yb_xZr_2O_7$ (x=0-2.0) transparent ceramics exhibit efficient upconversion photoluminescence emission in the visible wavelength region at 524 nm, 541 nm, 650 nm and downconversion emission at 1525 nm, 1565 nm, 1646 nm.

Keywords: transparent ceramics, luminescence, energy transfer, $Er_{2-x}Yb_xZr_2O_7$.

1. Introduction

In recent years, pyrochlore transparent ceramic has received a high degree of attention and

widespread concern from researchers in many different fields because of its unique and excellent properties. Pyrochlore ceramics exhibit the advantages of high melting point, good chemical stability, good ionic conductivity, low thermal conductivity and high catalytic activity. Therefore, these compounds exhibit various application prospects, such as thermal barrier coatings, solid oxide fuel cells, catalysts, scintillator matrix materials, nuclear waste solidification, solid laser materials and other fields [1-6]. The general formula of pyrochlore is $A_2B_2O_7$, in which A is generally trivalent cation (lanthanide element and Y element) while B is tetravalent cation (usually Zr, Hf, Ti) [7-11]. The structure depends on the radius ratio and temperature of the rare earth cation and anion. Some studies have pointed out that it indicates the disordered defective fluorite structure when r_A/r_B <1.46 [12]. When $1.46 \leq r_A/r_B \leq 1.78$, it shows the ordered pyrochlore structure. It is the monoclinal structure when $r_A/r_B > 1.78$. Because the structures of pyrochlore (space group: Fd-3M) and defective fluorite (space group: Fm-3m) are cubic systems, ceramics with these structures can be make transparent by solid-state sintering in vacuum.

The rare earth ions show extremely complex linear spectra. Different matrix materials can make rare earth ions in different spatial distribution, different coordination environment and different transfer efficiency, so that they have different luminescence properties [13]. The Er^{3+} ion is an ideal up-conversion activator ion. They have a stepped distribution of energy levels, longer lifetime and appropriate energy level spacing. But Er^{3+} ion has poor absorption capacity and small absorption cross section. Therefore, the conversion rate of Er^{3+} ions is usually improved by adding sensitizers [14]. Yb^{3+} is an ion that has only one excited energy level. In the case of high concentration doping, it has a certain tolerance and will not decrease the luminescence intensity due to the cross relaxation process [15]. At the same time, Yb^{3+} ion has no excited state absorption

and is beneficial to the application of high density excitation. The combination of Er^{3+} and Yb^{3+} enhances the emission intensity of Er^{3+} due to the high absorption cross section of Yb^{3+} and Eb^{3+}, and the energy is effectively transferred from Yb^{3+} to Er^{3+}. Therefore, Yb^{3+} - Er^{3+} co-doped materials have attracted much attention. In recent years, researchers have made many explorations such as $SrLaGa_3O_7$:Er/Yb, $NaBiF_4$:Yb/Er, β-$NaYF_4$: Er/Yb, Yb/Er:YAG, $Y_2Sn_2O_7$:Yb^{3+}/Er^{3+} [16-20].

Optical elements with high doping density and morphology can be obtained by ceramic technology. Ji et al. have successfully prepared transparent $La_2Hf_2O_7$ ceramic with maximum in-line transmittance higher than 70% by vacuum sintering [21]. Wang et al. have successfully prepared $La_{2-x}Lu_xZr_2O_7$ (x = 0-2.0) transparent ceramics by solid-state reactive sintering in vacuum [22]. It can be found that phase transition from pyrochlore to defective fluorite occurred with the increase of Lu content (x). Zhao et al. have successfully synthesized $La_{2-x}Gd_xZr_2O_7$ (x=0-2.0) transparent ceramics [23]. The x = 1.0, 1.2 and 1.6 samples exhibit high optical transmittance in the 450 nm-600 nm range and the $La_{0.4}Gd_{1.6}Zr_2O_7$ sample shows the highest transmittance of 83.84%. The transparent $Gd_{2-x}Nd_xZr_2O_7$ (x=0.4-2.0) ceramics were successfully prepared by Li et.al, in which the highest transmittance can reach to 78% at 1000 nm when x = 0.4 [24]. The aim of this work is to fabricate $Er_{2-x}Yb_xZr_2O_7$ (x=0.4-2.0) transparent ceramics with high optical quality. We attempt to explore the effects of Er-Yb with different contents on the luminescence performance of ceramics and the possibility of its use as laser material and upconversion material. The preparation technique, morphology, crystal structure and transmittance of the powders and final transparent ceramics were investigated.

2. Experimental procedure

2.1 Fabrication of $Er_{2-x}Yb_xZr_2O_7$ (x=0.4-2.0) transparent ceramics

Erbium nitrate ($Er(NO_3)_3 \cdot 6H_2O$, 99.9%, Aladdin industrial Co. ltd.), Ytterbium nitrate ($Yb(NO_3)_3 \cdot 6H_2O$, 99.9%, Aladdin industrial Co. ltd.), Zirconium nitrate ($Zr(NO_3)_4 \cdot 5H_2O$, 99.9%, Aladdin industrial Co. ltd.) and glycine were employed as the raw reactants. Firstly, the stoichiometric amounts of the four ingredients were dissolved in deionized water and stirred to clarified state. Appropriate amount of ammonia was slowly added to the mixture until the pH was adjusted to 4. Then, the solution was heated in a water bath until the solution changed to a sol-gel state. After that, it was transferred to a muffle furnace and then calcined at 300 °C in air to obtain fluffy powder. Subsequently, the primary fluffy powders were calcined at 1200 °C for 2 h and then ball milled in deionized water for 24 h with water as the medium. The ball milled slurry was sieved, dried and preformed into thin discs. Finally, the samples were vacuum sintered at 1850 °C for 6 h and annealed at 1500 °C for 5 h in air. The obtained ceramic samples were double-side polished to a thickness of 1 mm for subsequent tests.

2.2 Characterizations

The phase composition and crystal structure of the calcined powders and final ceramic samples were measured by X-ray diffractometer (XRD, X' Pert PRO, PANalytical B.V., Netherlands). The thermal-etched surface and the fracture surface of transparent ceramics were observed by scanning electron microscopy (SEM, Quanta 450F, FEI, USA), where the back-scattered electron (BSE) mode was conducted to analyze the grain sizes. The elemental distribution was measured using energy dispersive X-ray spectrometer (EDX) attached with the SEM equipment. The transmittance spectra of final ceramics were measured by solid ultraviolet–visible spectrophotometer (UV-VIS, Solidspec-3700, Shimadzu, Japan). The

luminescence spectra were characterized at room temperature by the OMN15015i spectrometer (Zolix, China), iHR 320 spectrometer (Jobin-Yvon, France) and 980 nm laser diode (LD, LEO photoelectric, China).

3. Results and discussion

3.1 XRD analysis of $Er_{2-x}Yb_xZr_2O_7$ (x=0-2.0) powders and ceramics.

The crystal structure of $Er_{2-x}Yb_xZr_2O_7$ (x = 0-2.0) powders calcined at 1200 °C for 3 h were characterization by XRD and the results are shown in Fig. 1. Due to the low calcination temperature, all the diffraction peaks are not sharp and it shows insufficient crystallinity degree. It is found that the phase structure is basically the same although the composition of ceramics is different. It may be due to the ionic radii of Er^{3+} (89 p.m.), Yb^{3+} (87 p.m.) are similar. The position of the peak in the doped sample does not change with the doping concentration, which indicate that the doping concentration had no influence on the matrix structure. According to the the M.A. Subramanian's theory, all the ceramics exhibit the defective fluorite structure [12].

Fig. 2 shows XRD patterns of the polished $Er_{2-x}Yb_xZr_2O_7$ (x=0-2.0) ceramics. Compared with the calcined powders, the obtained ceramics are much better crystallized after sintering as shown in Fig. 2. The full width at half maximum (FWHM) of XRD diffraction peaks decreases, which indicates that grain growth occurs during high temperature sintering. It can be seen that the diffraction peaks position are in agreement with the main (111), (200), (220) and (311) peaks of the $ErYbZr_2O_7$ ceramic. In contrast to the powders, the (222), (400) peaks of the $Er_{2-x}Yb_xZr_2O_7$ (x=1.2, 1.6, 2.0) ceramics take on different forms, which may due to the different orientation of ceramic grains. In addition, all diffraction peaks are sharp and the crystallinity of powders are high due to high calcination temperature and long holding time (1200 °C, 2 h).

3.2 Morphology and energy spectrum analysis of $Er_{2-x}Yb_xZr_2O_7$ (x=0.4-2.0) ceramics

Fig. 3 shows the back-scattered electron images of the thermal etched surface of ceramics x=0.4-2.0. It can be seen from these photographs that all ceramics present dense microstructures and the grain size is about 100 μm. There are many pores in ceramics, which are the most important factors affecting the transparency of ceramics. Because the ceramics in this study are all in single cubic defective fluorite structure, the main factor affecting the transparency of ceramics is residual porosity. Micropores in transparent ceramics may exist at grain boundaries and within grains. The porosity of grain boundary can be eliminated with the migration of grain boundary, but it is difficult to eliminate the intracrystalline hole. In order to avoid the formation of pores in the grain, the sintering process must be controlled so that the moving rate of grain boundary is not too fast and the pores are not allowed to enter the grains. Pore size also plays an important role on the transmittance of ceramics [25, 26]. The fracture surfaces of $Er_{2-x}Yb_xZr_2O_7$ (x=0.4-2.0) ceramics are presented in Fig. 4. The microstructure images demonstrate that the fracture surfaces are mostly in transgranular mode other than intergranular mode, which indicates that the bonding strength of grain boundary is relatively high and the internal stress is low. A considerable number of pores can be found in the grains of x=0.4-2.0. These intragranular pores were formed during the final ceramics were thermal etched in a muffle furnace at 1500 °C for 5h.

Elemental compositions are analyzed by elemental energy spectrum in Fig. 5. $ErYbZr_2O_7$ transparent ceramic exhibits two different grayscales from the back-scattering diagram, which shows obvious element enrichment phenomenon. Through the point-sweep analysis of energy spectrum, it is found that there are more Er elements in the darker area and more Yb elements in the lighter area. But the element content difference formed in this situation is not significant. To

further verify this result, two points of spectrum 1 and spectrum 2 in Fig. 5(a) are further characterized using EDX elemental spotting analysis with the results listed in Fig. 5(b). The Er/Yb ratio of two points are 1.07:1 and 1:1.09, which all are close to 1:1. Studies on $LaLuZr_2O_7$ ceramics prepared by Z.J. Wang and $La_{1.28}Er_{1.28}Zr_2O_7$ ceramics prepared by W.W. Zhao found that differences in atomic radius ratio and element content resulted in the formation of both defective fluorite and calcite phases [27,28]. Two different phases are obviously observed in different grayscale. However, $ErYbZr_2O_7$ ceramics have a single missing fluorite phase, so two different grayscales have nothing to do with the phase structure. It may be because Er and Yb have different atomic radii, which make it impossible for the elements to be evenly distributed in $ErYbZr_2O_7$ ceramics. Moreover, the enrichment of Er or Yb elements is small due to the close atomic radii of Er and Yb.

3.3 Optical performance analysis

The illustration in Fig. 6 shows the macroscopic photos of $Er_{2-x}Yb_xZr_2O_7$ (x=0-2.0) transparent ceramics. All the samples exhibit excellent transmittance in the visible region and the text under the samples can be clearly seen. In-line optical transmittances of $Er_{2-x}Yb_xZr_2O_7$ ceramics were tested with the results shown in Fig 6. It should be mentioned that all the samples exhibit near infrared transmittance higher than 70%, where the highest transmittance can reach to 76% at 1100 nm when x=0. The sample shows the lowest transmittance reach to 70% when x = 0.4, which may be due to the presence of pores. Many absorption peaks can also be observed in the transmittance curve, which are located at the wavelength range from 200 nm to 2000 nm. The x=2.0 sample exhibit absorption peaks at 913 nm and 980 nm, which are related to the level excitation of Yb^{3+} from $^2F_{7/2}$ to $^2F_{5/2}$ in 4f-4f. Absorption bands lying at 350-1000 nm wavelength

range correspond to transition from $^4I_{15/2}$ ground level of Er^{3+} ions to the $^2H_{9/2}$, $^4F_{7/2}$, $^2H_{11/2}$ and $^4S_{3/2}$ upper levels, while those at 1400–1650 nm correspond to $^4I_{15/2} \rightarrow {}^4I_{13/2}$ transitions [29-33].

Efficiency of $Yb^{3+} \rightarrow Er^{3+}$ resonant energy transfer during sensitized luminescence strongly depends on the concentration ratio of involved ions. Comparison of luminescence intensity of some spectral lines in ceramic samples containing different Yb/Er ratio allows us to study the influence of Er^{3+} concentration on luminescent properties of ceramics. Fig. 7 shows the upconversion luminescence (UCL) spectra of $Er_{2-x}Yb_xZr_2O_7$ (x=0-2.0) transparent ceramics in the 500-750 nm region under 980 nm excitation. All spectra show two characteristic bands of Er^{3+} in 500-750 nm region. The bright green and red luminescence of the samples can be observed. The peaks in the green region of 510-540 nm and 544-580 nm are attributed to the $^2H_{11/2} \rightarrow {}^4I_{15/2}$ and $^4S_{3/2} \rightarrow {}^4I_{15/2}$ transitions of Er^{3+} ions while the peaks in the red region of 625–720 nm can be assigned to the $^4F_{9/2} \rightarrow {}^4I_{15/2}$ transition [34, 35]. And the intensity of red luminescence is significantly higher than that of green luminescence. It is noted that the emission spectra of x=0 and x = 2.0 samples present no peaks in upconversion luminescence spectrum. The x = 1.0 and x = 1.6 samples demonstrate basically the same peak shape and peak strength in green area. The x = 1.6 sample exhibits the highest luminescence intensity in the red region.

Fig. 8 presents the near-infrared emission spectra of the $Er_{2-x}Yb_xZr_2O_7$ (x=0-2.0) ceramics in the 1400-1700 nm range under 980 nm wavelength excitation. The luminescence lines with the peaks at approximately 1525 nm, 1565 nm and 1646 nm correspond to the $^4I_{13/2} \rightarrow {}^4I_{15/2}$ transition of Er^{3+} ion. The x=0.4 and x=0.8 samples have similar luminescence intensity. The luminescence intensities at 1525 nm in the sample of x = 1.0 is lower than in that the sample of x=1.6. And the fluorescence intensity gradually increases as x increases from 1.0 to 1.6. It shows the highest

luminescence intensities at x=1.6, which is due to the increase of Yb^{3+} concentration shortens the average distance between Yb^{3+} and Er^{3+} ions. Broad emission bandwidths are advantageous for tunable laser output and make $Er_{0.4}Yb_{1.6}Zr_2O_7$ transparent ceramic a promising 1.5 μm solid-state tunable laser media.

Fig. 9 shows the energy level diagram of Er^{3+}/Yb^{3+} ions and the possible energy transfer fluorescence mechanism of the ceramics. The electron of Yb^{3+} ions jumping from ground level ($^2F_{7/2}$) to excited level ($^2F_{5/2}$) when the $Er_{2-x}Yb_xZr_2O_7$ (x =0-2.0) transparent ceramics were pumping by 980 nm laser. Then, energy transfer occurs between Yb^{3+} ions and nearby Er^{3+} ions due to the electron populated in $^2F_{5/2}$ is not stable. The excited states of Er^{3+} for upconversion emission include energy transfer (ET) and ground/excited state absorption (GSA/ESA). The specific process is as follows: the Yb^{3+} ions at $^2F_{7/2}$ state undergo a transition to its $^2F_{5/2}$ state by absorbing one 980 nm photon, release energy in the form of photon, adjacent Er^{3+} capture this photon and jump from $^4I_{15/2}$ to $^4I_{11/2}$ simultaneously. On the one hand, multi-phonon relaxes from $^4I_{11/2}$ to $^4I_{13/2}$ state. After receiving the energy equal to a 980 nm photon from the Yb^{3+} ions, the Er^{3+} ions jump from $^4I_{13/2}$ to $^4F_{9/2}$. On the other hand, the Er^{3+} ions populated in $^4I_{11/2}$ capture another photon from Yb^{3+} ion jump to the $^4F_{7/2}$ level state with more higher energy. However, electrons located in excited $^4F_{7/2}$ state is not stable. And part of energy would be lost by non-radiative relaxation as the electron jumped to $^4S_{3/2}$, $^2H_{11/2}$, $^4F_{9/2}$. Radiative transition of $^2H_{11/2}/^4S_{3/2} \rightarrow {}^4I_{15/2}$ of Er^{3+} ions generate green UCL emissions of the ceramics. The electrons populated in $^4F_{9/2}$ would jump to ground state of $^4I_{15/2}$ and release energy by emitting red light. Radiative transition of $^4I_{13/2} \rightarrow {}^4I_{15/2}$ generate near infrared emission at around 1526 nm, which is useful in many fields, especially for near infrared laser applications and optical communication.

4. Conclusions

$Er_{2-x}Yb_xZr_2O_7$ (x=0-2.0) transparent ceramics were successfully fabricated by vacuum sintering at 1850 °C for 6h. All the ceramics exhibit the defective fluorite structure and the grain size is about 100 μm. All the samples are transparent and the highest in-line transmittance is 76% when x=1.0. The ceramics exhibite green and red upconversion emission, as well as broad-bandwidth near-infrared emission. The intensity of red luminescence is significantly higher than that of green luminescence. This study confirms that the $Er_{2-x}Yb_xZr_2O_7$ (x =0-2.0) transparent ceramics are promising optical material with efficient visible upconversion and downconversion photoluminescence properties.

Acknowledgements

We sincerely appreciate the projects supported by the National Natural Science Foundation of China (Grant No. 51672228) and the Project of State Key Laboratory of Environment-friendly Energy Materials (Southwest University of Science and Technology, 17FKSY0104 and 18FKSY0214).

References

[1] Wang J, Bai SX, Zhang H, Zhang CR. The structure, thermal expansion coefficient and sintering behavior of Nd^{3+}-doped $La_2Zr_2O_7$ for thermal barrier coatings. *J Alloy Comp* 2009, **476**: 89-91.

[2] Martínez-Coronado RA, Aguadero C, Calle DL. Evaluation of the R_2RuMnO_7 pyrochlores as cathodes in solid-oxide fuel cells. *J Power Sources* 2011, **196**: 4181-4186.

[3] Tong YP, Xue PP, Jian FF, Lu LD, Wang X, Yang XJ. Preparation and characterization of $Y_2Zr_2O_7$ nanocrystals and their photocatalytic properties. *Mater Sci Eng* 2008, **150**: 194-198.

[4] Zhao WW, Zhang KB, He ZS, Xue JL, Li WW, Xie DY, Zhang HB. Vacuum sintering of highly transparent $La_{1.28}Yb_{1.28}Zr_2O_{7.84}$ ceramic using nanosized raw powders. *Ceram Int* 2018, **44**: 12535-12538.

[5] Zhang KB, He ZS, Peng L, Zhang HB, Lu XR. Self-Propagating synthesis of $Y_{2-x}Nd_xTi_2O_7$ pyrochlore and its aqueous durability as nuclear waste form. *Scr Mater* 2018, **146**: 300-303.

[6] Feng T, Clarke DR, Jiang DY, Xia JF , Shi JL. Neodymium zirconate ($Nd_2Zr_2O_7$) transparent ceramics as a solid state laser material. *Appl Phys Lett* 2011, **98**: 291.

[7] Mandal BP, Garg N, Sharma SM, TyagiPreparation AK. XRD and Raman spectroscopic studies on new compounds $RE_2Hf_2O_7$ (RE=Dy, Ho, Er, Tm, Lu, Y): pyrochlores or defect-fluorite? *J Solid State Chem* 2006, **179**: 1990-1994.

[8] Liu ZG, Y. Zhou, et al. Heat capacity measurements on $Yb_xGd_{2-x}Zr_2O_7$ (x=0, 1, 2) ceramics by differential scanning calorimetry. *Bull Mater Sci* 2009, **32**: 603-606.

[9] Whittle KR, Cranswick L, Redfern SA, et al. Lanthanum pyrochlores and the effect of yttrium addition in the systems $La_{2-x}Y_xZr_2O_7$ and $La_{2-x}Y_xHf_2O_7$. *J Solid State Chem* 2009, **182**: 442-450.

[10] Zhang HS, Sun K, Xu Q, Wang F, Liu L. Thermal conductivity of $(Sm_{1-x}La_x)_2Zr_2O_7$ (x=0, 0.25, 0.5, 0.75 and 1) oxides for advanced thermal barrier coatings. *J Rare Earth* 2009, **27**: 222-226.

[11] Zhang FX, Wang JW, Lian J, Lang MK, Becker U, Ewing RC. Phase stability and pressure dependence of defect formation in $Gd_2Ti_2O_7$ and $Gd_2Zr_2O_7$ pyrochlore. *Phys Rev Lett* 2008, **100**: 045503.

[12] Subramanian MA, Aravamudan G, Subba Rao GV. Oxide Pyrochlores–A Review, Prog. *Solid State Chem* 1983, **15**: 55-143.

[13] Dong H, Sun L, Yan C. Energy transfer in lanthanide upconversion studies for extended optical applications. *Chem Soc Rev* 2015, **44**: 1608.

[14] Tikhomirov VK, Rodriguez VD, Mendez-Ramos J, et al. Optimizing Er/Yb ratio and content in Er–Yb co-doped glass-ceramics for enhancement of the up- and down-conversion luminescence. *Sol Energ Mat Sol C* 2012, **100**: 209-215.

[15] Fei B, Chen W, Guo W, Shi M, Lin H, Huang Q, Zhang G, Cao Y. Optical properties and laser oscillation of Yb^{3+}, Er^{3+} co-doped $Y_3Al_5O_{12}$ transparent ceramics. *J Alloy Compd* 2015, **636**: 171-175.

[16] Voiculescu AM, Tihon CE, Hau Ş, Stanciu G, Toma O. Optical study of $SrLaGa_3O_7$ ceramic samples doped with $Er^{3+}$and Yb^{3+}. *Opt Mater* 2020, **100**: 109613.

[17] Fu J, Hu XW, Luan FF, Li GZ, Guo DC. Optimum synthesis and properties of $NaBiF_4$:Yb /Er upconversion nanoparticles. *Ceram Int* 2019, **45**: 24365-24374.

[18] DungCao TM, GiangLe TT, NhungNguyen TP, NguyetDau TA, et al. Investigating the effect of Yb^{3+} and $Er3^{+}$ concentration on red/green luminescent ratio in β-$NaYF_4$: Er, Yb nanocrystals using spectroscopic techniques. *J Molecular Struc* 2020, **1210**: 128014.

[19] Vorona IO, Yavetskiy RP, Dobrotvorskaya MV, Doroshenko AG, Parkhomenko SV, et al. 1532 nm sensitized luminescence and up-conversion in Yb,Er:YAG transparent ceramics. *Opt Mater* 2018, **77**: 221-225.

[20] Liao J, Nie L, Liu S, Liu B, Wen H. Yb^{3+} concentration dependence of up conversion luminescence in $Y_2Sn_2O_7$:Yb^{3+}/Er^{3+} nanophosphors. *J Mater Sci* 2014, **49**: 6081-6086.

[21] Ji YM, Jiang DY, Tao F. Fabrication of transparent $La_2Hf_2O_7$ ceramics from combustion synthesized powders. *Mater Res Bull* 2005, **40**: 553-559.

[22] Wang ZJ, Zhou GJ, Qin XP. Fabrication and phase transition of $La_{2-x}Lu_xZr_2O_7$ transparent ceramics. *J Eur Ceram Soc* 2014, **34**: 3951–3958.

[23] Li WW, Zhang KB, Xie DY, Deng T, Zhang HB, Huang XG. Solid-state reactive sintering of $La_{2-x}Gd_xZr_2O_7$ transparent ceramics and their optical properties. *Ceram Int* 2019, **45**: 20078-20083.

[24] Li WW, Zhang KB, Xie DY, Deng T, Zhang H.B, Huang XG. Vacuum sintering and optical properties of $Gd_{2-x}Nd_xZr_2O_7$ transparent ceramics using combustion synthesized nanopowders. *Opt Mater* 2020, **100**: 109622.

[25] Rolf A, Van Bruggen MPB. Transparent alumina: a light-scattering model. *J Am Ceram Soc* 2003, **86**: 480-486.

[26] Ikesue A, Yoshida K. Influence of pore volume on laser performance of Nd:YAG ceramics. J Mater Sci 1999, **34**: 1189-1195.

[27] Zhao WW, Zhang KB, Li WW. Fabrication and optical properties of transparent $LaErZr_2O_7$ ceramic with high excess contents of La and Er. *Ceram Int* 2019, **45**: 11717-11722.

[28] Wang ZJ, Zhou GH, Qin XP. Two-Phase $LaLuZr_2O_7$ transparent ceramic with high transparency. *J Am Ceram Soc* 2014, **97**: 2035-2037.

[29] Mao YB, Tran T, Guo X, Huang JY, Shih CK, Wang KL, Chang JP. Luminescence of nanocrystalline erbium-doped yttria. *Adv Funct Mater* 2009, **19**: 748-754.

[30] Vetrone F, Boyer JC, Capobianco JA, Speghini A, Bettinelli M. Significance of Yb^{3+} concentration on the upconversion mechanisms in codoped $Y_2O_3:Er^{3+}$, Yb^{3+} nanocrystals. *J Appl. Phys* 2004, **96**: 661-667.

[31] Cao BS, He YY, Zhang L, Dong B. Upconversion properties of Er^{3+}-Yb^{3+}:$NaYF_4$ phosphors with a wide range of Yb^{3+} concentration. *J Lumin* 2013, **135**: 128-132.

[32] Guo H, Qiao YM. Preparation, characterization, and strong upconversion of monodisperse Y_2O_3:Er^{3+},Yb^{3+} microspheres. *Opt Mater* 2009, **31**: 583-589.

[33] Yang J, Zhang CM, Peng C, Li CX, et al. Controllable red, green, blue (RGB) and bright white upconversion luminescence of Lu_2O_3: Yb^{3+}/Er^{3+}/Tm^{3+}nanocrystals through single laser excitation at 980 nm. *Chem Eur J* 2009, **15**: 4649-4655.

[34] Chen X, Wu Y, Wei N, Qi J, Li Y, Zhang Q, et al. Fabrication and spectroscopic properties of Yb/Er:YAG and Yb, Er:YAG transparent ceramics by co-precipitation synthesis route. *J Lumin* 2017, **188**: 533-540.

[35] Harvey EJ, Whittle KR, Lumpkin GR, Smith RI, Redfern SA. Solid solubilities of $(La,Nd)_2(Zr,Ti)_2O_7$ phases deduced by neutron diffraction. *J Solid State Chem* 2005, **178**: 800-810.

Figure Captions:

Figure 1. XRD patterns of $Er_{2-x}Yb_xZr_2O_7$ (x=0-2.0) powders calcined at 1200 °C for 3 h.

Figure 2. XRD patterns of $Er_{2-x}Yb_xZr_2O_7$ (x=0-2.0) ceramics vacuum sintered at 1850 °C for 6 h and annealed at 1500 °C for 5 h in air.

Figure 3. Back-scattered electron (BSE) image of the $Er_{2-x}Yb_xZr_2O_7$ (x=0.4-2.0) ceramic thermal etched surface: (a) x=0.4 , (b) x=0.8, (c) x=1.0, (d) x=1.2, (e) x=1.6, (f) x=2.0.

Figure 4. Fracture surface images of the $Er_{2-x}Yb_xZr_2O_7$ (x=0.4-2.0) ceramics: (a) x=0.4, (b) x=0.8, (c) x=1.0, (d) x=1.2, (e) x=1.6 (f) x=2.0.

Figure 5. (a) Back-scattered electron (BSE) image of the $ErYbZr_2O_7$ transparent ceramic, (b) EDX spotting results of spectrum 1and spectrum 2.

Figure .6 The transmittance of mirror-polished $Er_{2-x}Yb_xZr_2O_7$ (x=0-2.0) transparent ceramics (1 mm in thickness). Illustration shows the macroscopic photo of $Er_{2-x}Yb_xZr_2O_7$ (x=0-2.0) transparent ceramics (1.0 mm thick).

Figure 7. Upconversion luminescence spectrum of $Er_{2-x}Yb_xZr_2O_7$ (x = 0-2.0) transparent ceramics when excited at 980 nm.

Figure 8. (a) The infrared emission spectra of $Er_{2-x}Yb_xZr_2O_7$ (x=0-2.0) transparent ceramics around 1525 nm under 980 nm excitation.

Figure 9. Level transition mechanisms of $Er_{2-x}Yb_xZr_2O_7$ (x=0-2.0) transparent ceramics under 980 nm laser pumping.

Figures

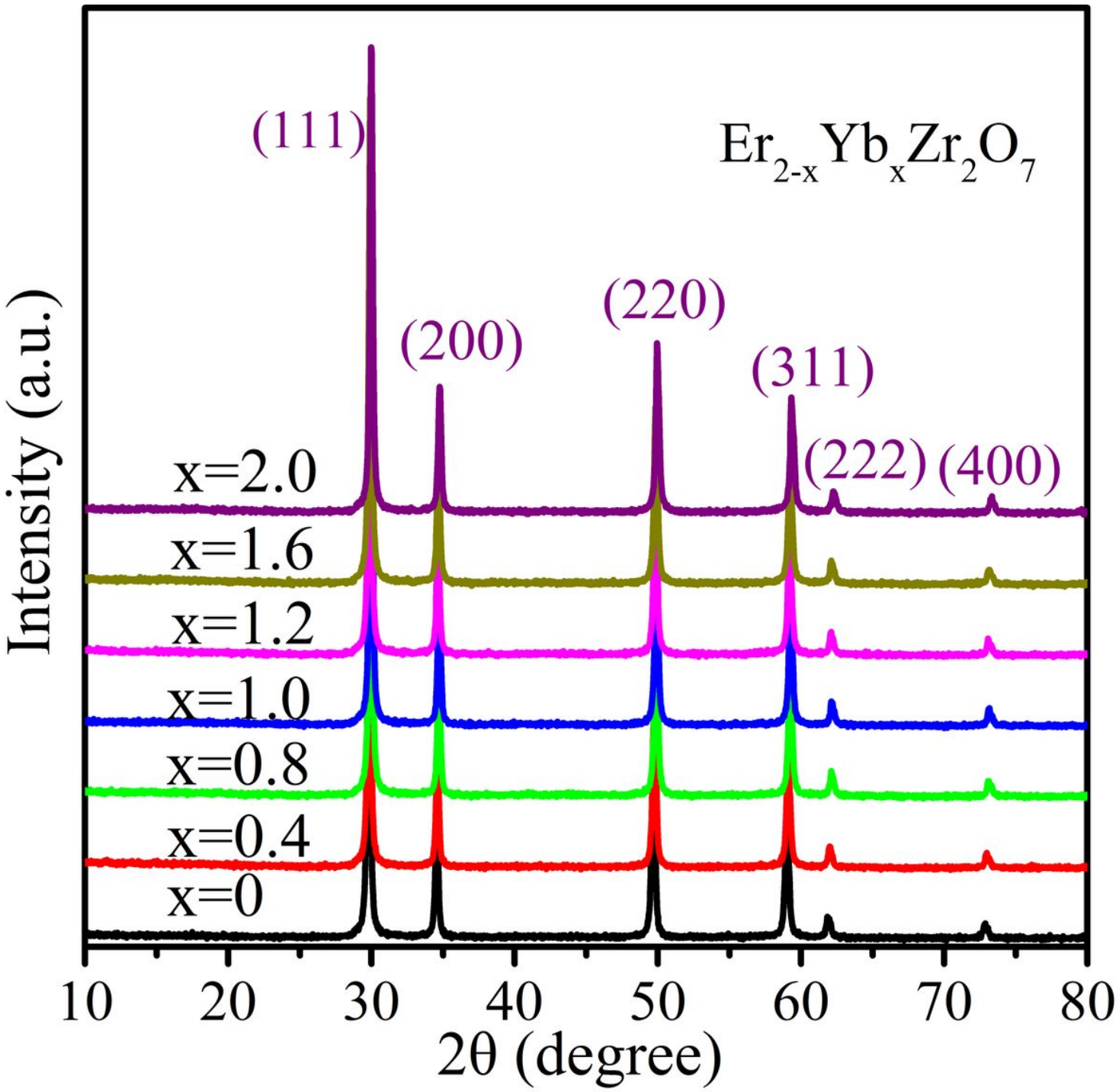

Figure 1

XRD patterns of Er2-xYbxZr2O7 (x=0-2.0) powders calcined at 1200°C for 3h.

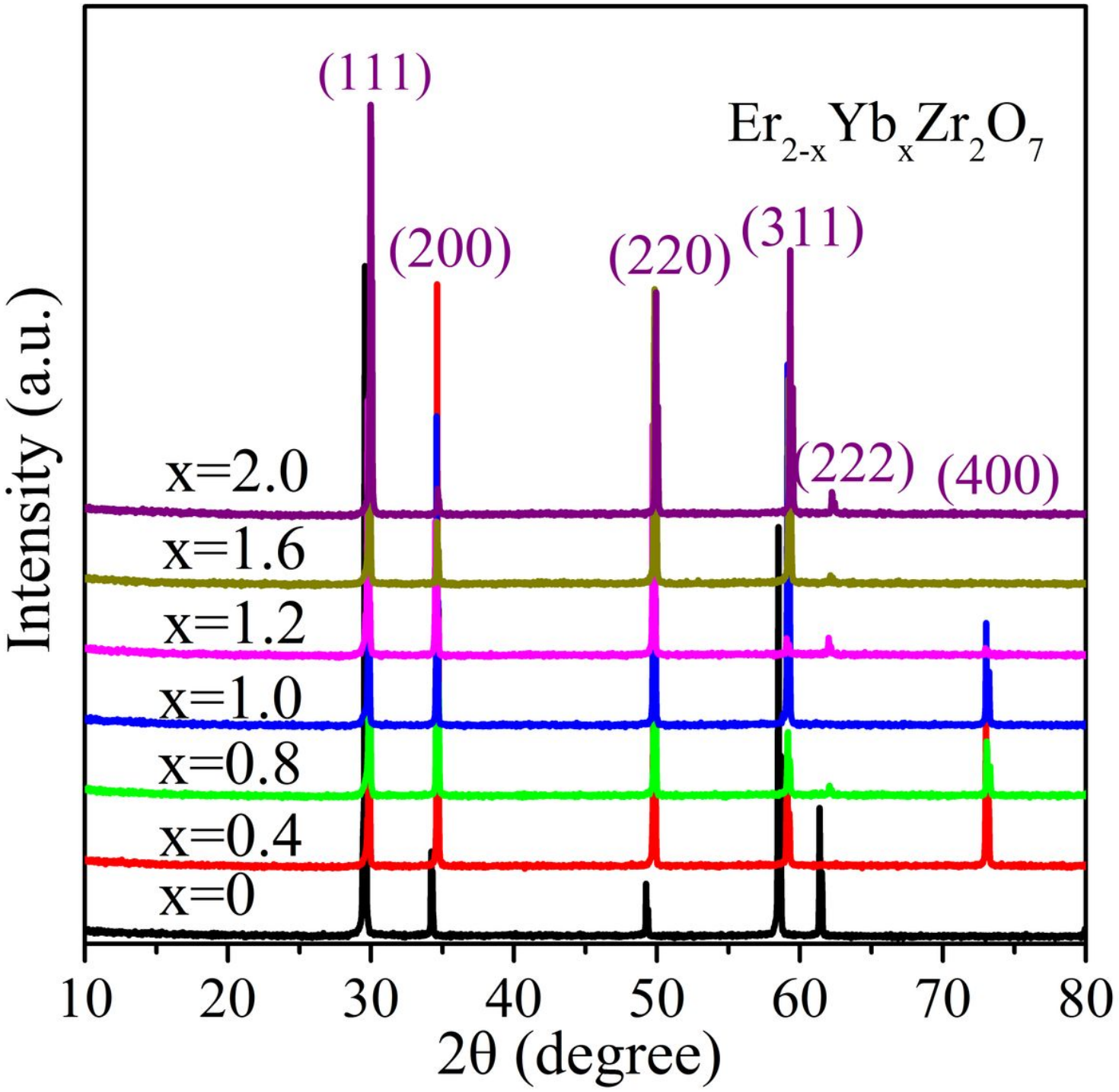

Figure 2

XRD patterns of Er2-xYbxZr2O7 (x=0-2.0) ceramics vacuum sintered at 1850 °C for 6 h and annealed at 1500°C for 5h in air.

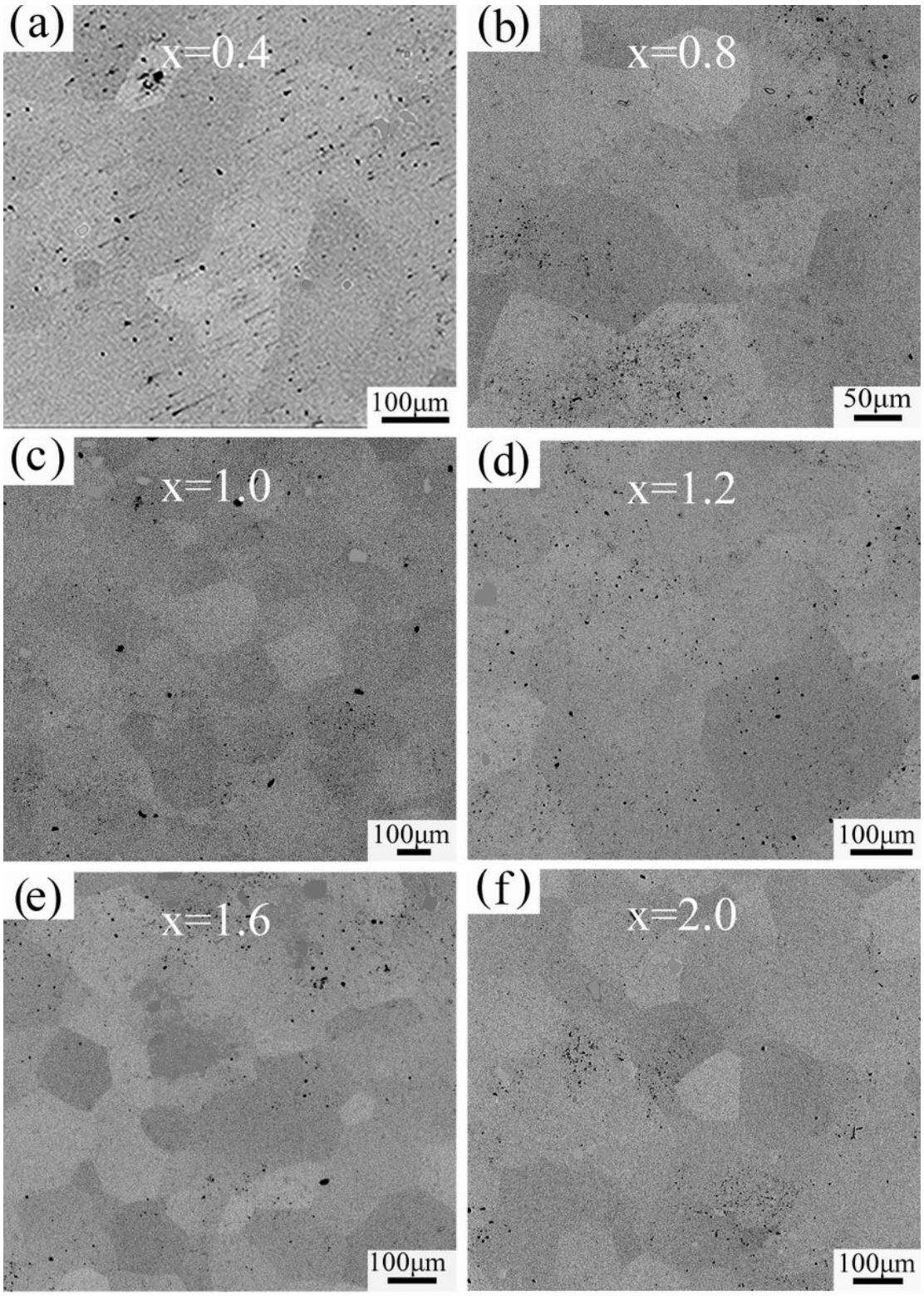

Figure 3

Back-scattered electron (BSE) image of the Er2-xYbxZr2O7 (x=0.4-2.0) ceramic thermal etched surface: (a)x=0.4,(b)x=0.8,(c)x=1.0,(d)x=1.2,(e)x=1.6,(f)x=2.0.

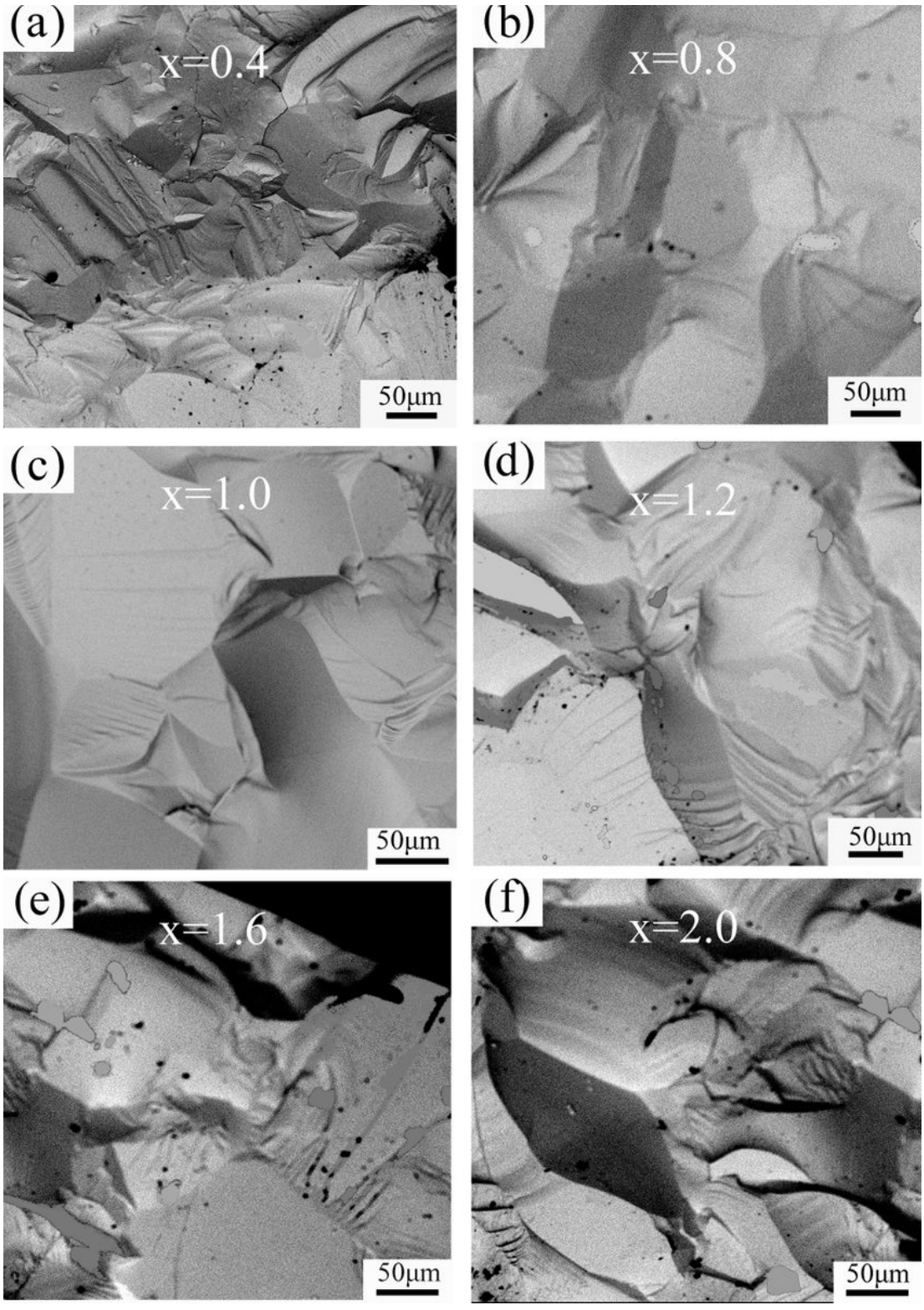

Figure 4

Fracture surface images of the Er2-xYbxZr2O7 (x=0.4-2.0) ceramics: (a) x=0.4, (b) x=0.8, (c)x=1.0, (d)x=1.2,(e)x=1.6(f) x=2.0.

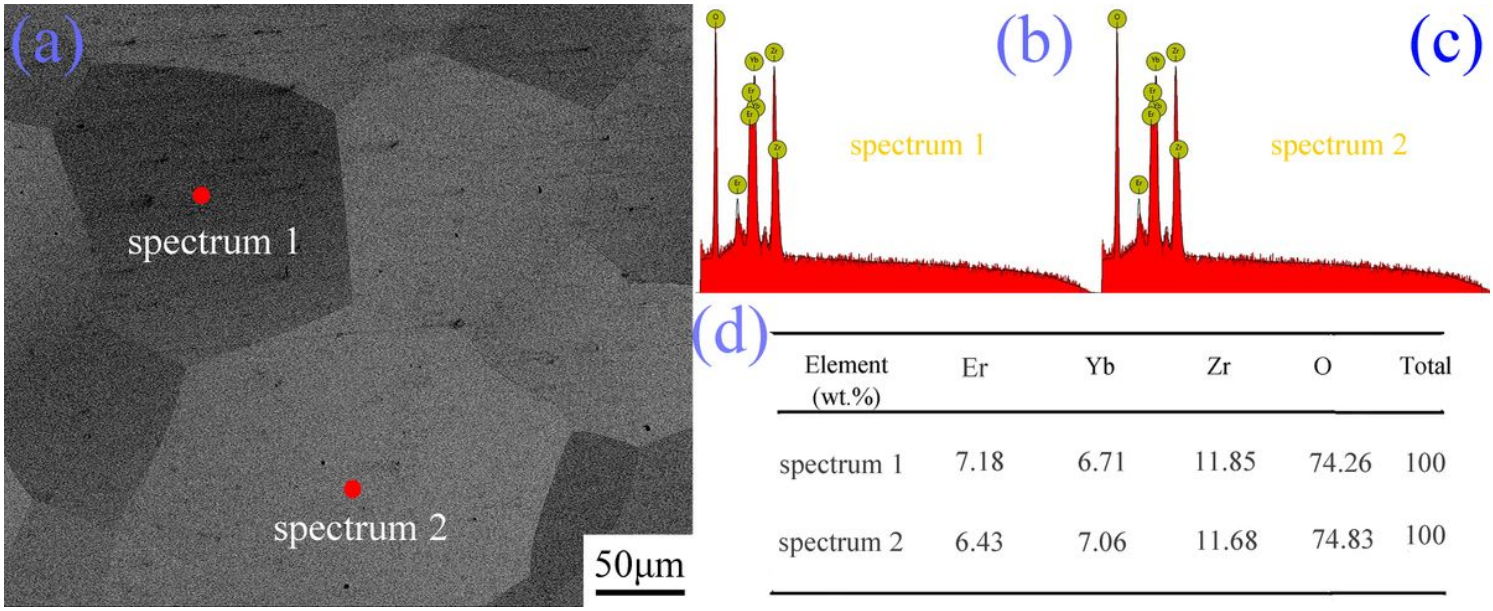

(d)

Element (wt.%)	Er	Yb	Zr	O	Total
spectrum 1	7.18	6.71	11.85	74.26	100
spectrum 2	6.43	7.06	11.68	74.83	100

Figure 5

(a) Back-scattered electron (BSE) image of the ErYbZr2O7 transparent ceramic, (b) EDX spotting results of spectrum 1 and spectrum 2.

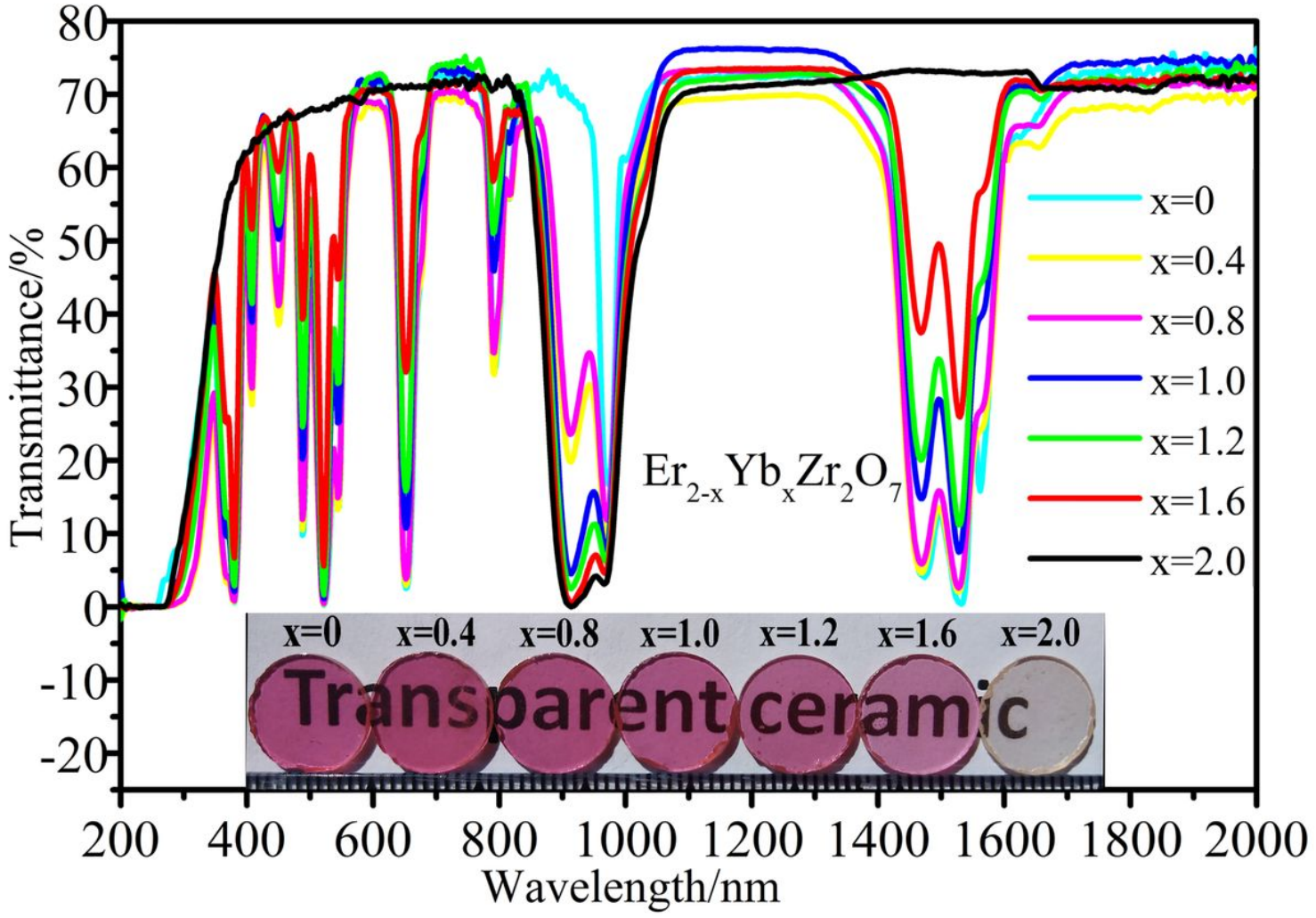

Figure 6

The transmittance of mirror-polished Er2-xYbxZr2O7 (x=0-2.0) transparent ceramics (1 mm in thickness). Illustration shows the macroscopic photo of Er2-xYbxZr2O7 (x=0-2.0) transparent ceramics(1.0mm thick).

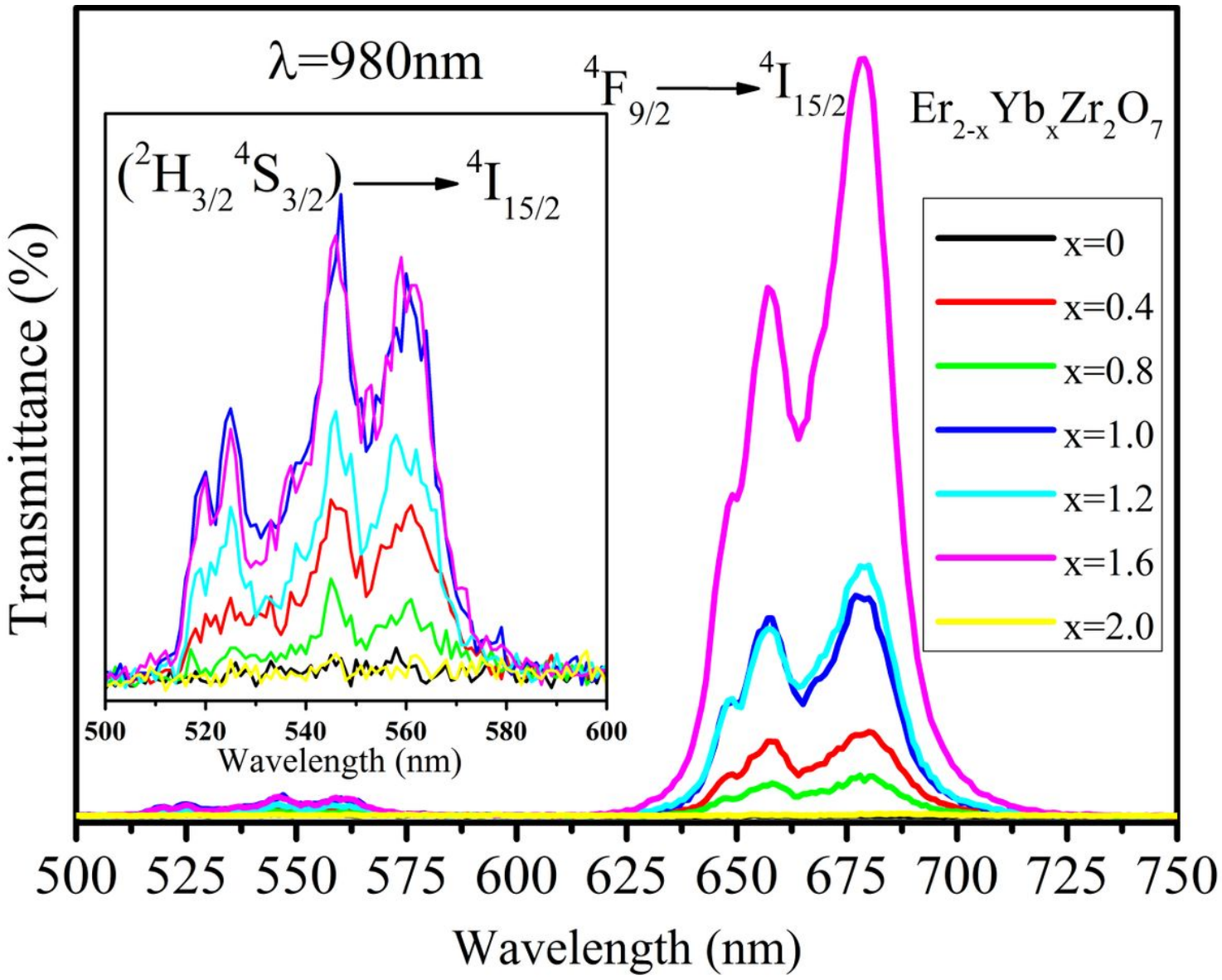

Figure 7

Upconversion luminescence spectrum of Er2-xYbxZr2O7 (x = 0-2.0) transparent ceramics when excited at 980 nm.

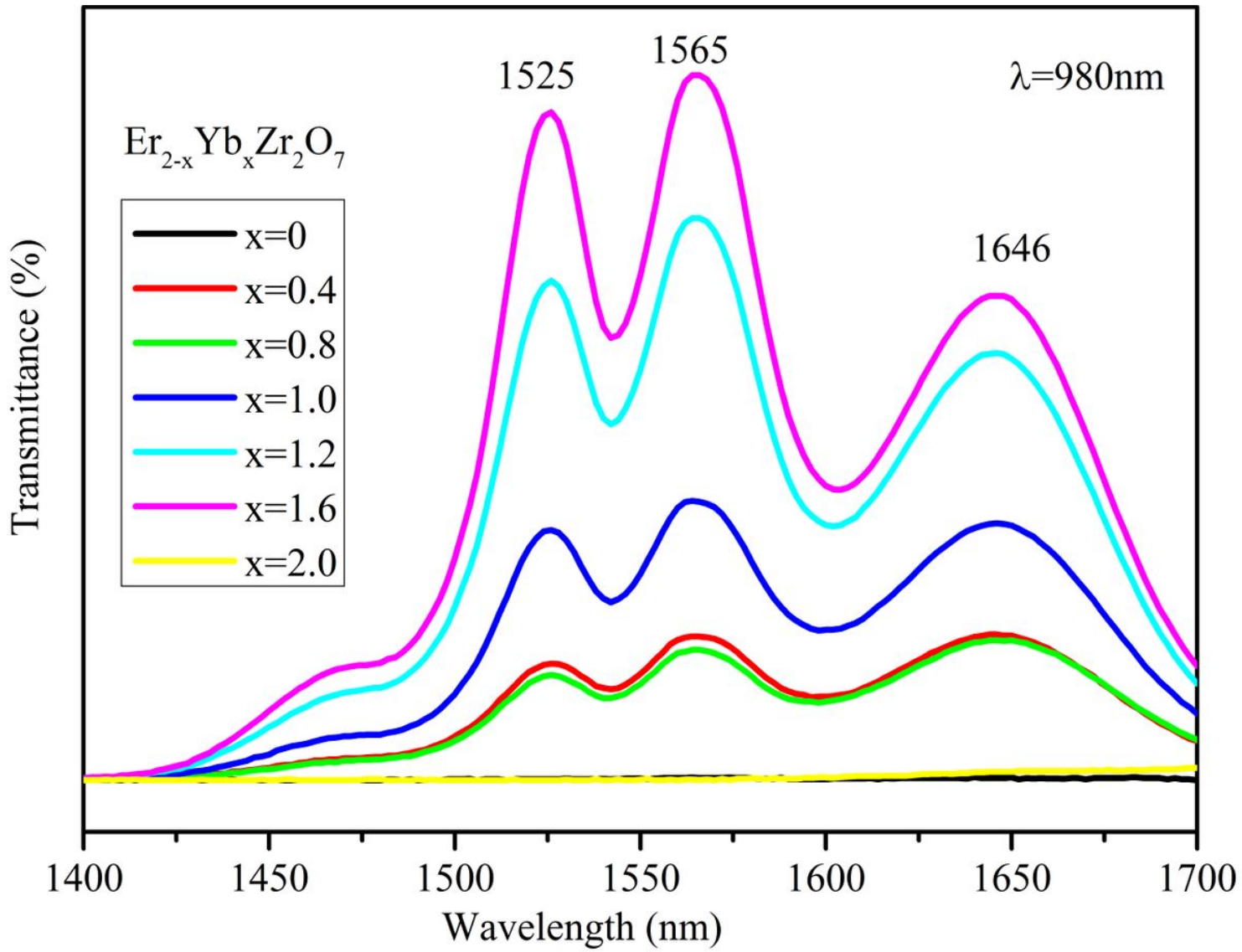

Figure 8

(a) The infrared emission spectra of Er2-xYbxZr2O7 (x=0-2.0) transparent ceramics around 1525 nm under 980 nm excitation.

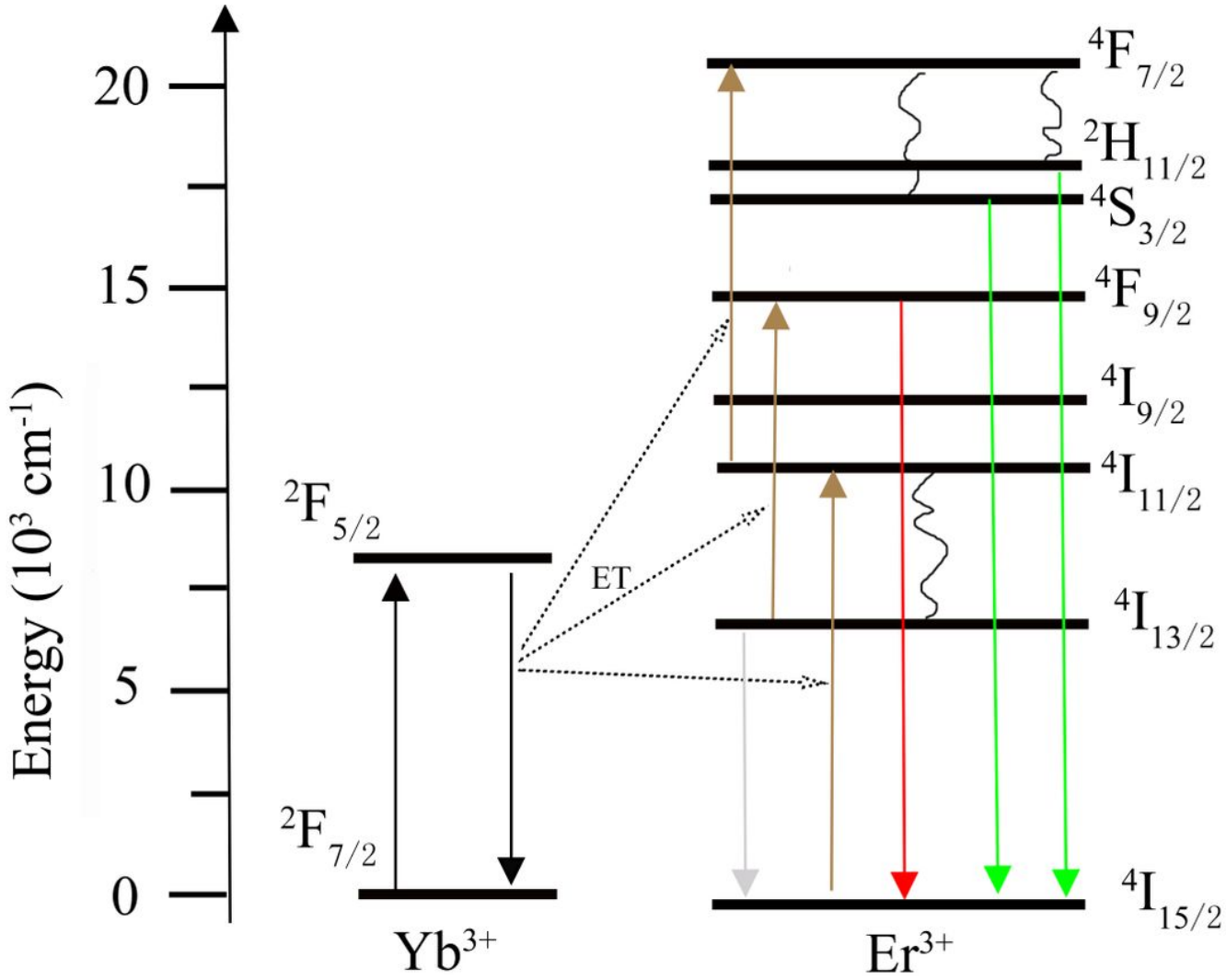

Figure 9

Level transition mechanisms of Er2-xYbxZr2O7 (x=0-2.0) transparent ceramics under 980 nm laser pumping.